Multiscale analysis and denoising of near offset Vibroseis data

Iga Pawelec and Paul Sava, Center for Wave Phenomena, Colorado School of Mines

SUMMARY

Seismic data are frequently acquired as long, continuous time series, but some of the benefits of this approach, such as improved time-frequency resolution and the ability to accurately quantify the noise, are oftentimes overlooked. Moreover, continuous time series facilitates access to low frequencies of the observed wavefields. Well-defined low frequencies are the key for impedance and full waveform inversions, while characterizing the noise background allows one to develop an effective denoising strategy, which in turn reduces the uncertainty of all seismic-derived products.

We demonstrate that the multiscale approach utilizing wavelet transforms is an efficient tool to quantify spatio-temporal characteristics of seismic data in different frequency bands. Our analysis uses a portion of finely-sampled continuous time data to characterize signal and noise present in near offsets of data acquired with a Vibroseis source. We find that the data generated by the baseplate coupling with the ground have better low frequency content than the sweep time data. We also identify and attenuate different types of noise, including acoustic and mechanical noise generated by the Vibroseis, harmonic distortion and powerline interference. We address the noise in the 2D complex wavelet domain, linking the bands and scales of the transform to the physical dimensions of seismic data and zeroing the coefficients corresponding to noise. The strategy presented in this paper is efficient for suppressing source-generated noise, surface waves and powerline interference, as demonstrated by comparing raw and denoised correlated data.

INTRODUCTION

Seismic acquisition has undergone many transformations over time with a singular goal in mind: getting the maximum information about earth's subsurface at the lowest cost. A good example of reducing the cost while maximizing the benefit is the blended acquisition (Bagaini, 2006; Berkhout, 2008; Abma et al., 2015). The underlying idea is to use multiple sources with some separation in time and space to increase the number of shot points and improve the illumination of the geological target. In the blended acquisition the data are recorded in continuous time and the energy corresponding to overlapping shots is separated during pre-processing, either through denoising or through sparse inversion.

With the advent of wireless acquisition systems, even non-blended surveys are recorded in continuous time. Wireless nodes record continuously for as long as they are deployed. This leads to an explosion of data which need to be stored, so often only the active survey pieces are kept. Is that the right approach to take? Or are we discarding a lot of potentially useful information? In this study we are looking at a portion of a continuous time recording to investigate what happens before, during and after vibroseis sweeps. Our experimental setup affords the examination of the finely sampled, near offset data that are of interest in surface related and Marchenko multiple elimination (Verschuur et al., 1992; Kabir and Verschuur, 1995; Zhang and Slob, 2020), multichannel analysis of surface waves (Xu et al., 2006), AVO attributes (Ross and Kinman, 1995) and of academic interest for the potential to observe non-linear wave behavior. We show that multiscale analysis allows to characterize spatio-temporal behavior of the recorded wavefields, providing important information about signal and noise.

The classification of noise depends on specific application of seismic data, but most commonly in exploration seismology reflected waves are of interest. All other wave phenomena present in seismic record are then considered noise and directly affect the uncertainty of seismic-derived products, including migrated images, attribute maps and models of physical properties. Understanding and suppressing the noise automatically reduces that uncertainty. We demonstrate that the mapping between the physical domain of seismic data and scales and bands of the 2D complex wavelet transform combined with the noise characteristics derived from multiband analysis of continuous time seismic data allows to efficiently suppress the majority of the source-generated and environmental noise, as well as surface waves.

METHODOLOGY

Time-frequency analysis

There exist an inherent trade-off between time and frequency resolution of a signal which is summarized by the Heisenberg uncertainty principle

$$\sigma_t^2 \sigma_\omega^2 \geq \frac{1}{4}, \tag{1}$$

where σ_t^2 and σ_ω^2 correspond to temporal and frequency variances, respectively. Let $\sigma_t \times \sigma_\omega$ define the Heisenberg box. The optimal choice for time-frequency representation of a signal depends on the prior knowledge of these characteristics. In seismic exploration high frequencies are preferentially attenuated, while well-defined low frequencies are important to applications such as acoustic impedance or full waveform inversions (Ghosh, 2000; Kapoor et al., 2005; Baeten et al., 2013). Time-frequency decomposition of a signal can be obtained by the windowed Fourier transform (Gabor, 1946) which uses a fixed time window and has the same resolution across the entire time-frequency plane, with a Heisenberg box defined by $\sigma_t \times \sigma_\omega$. The desire to understand the non-stationary nature of seismic signals with high resolution inspired the introduction of wavelet transforms in geophysics (Morlet et al., 1982a,b). The continuous wavelet transform (CWT) depends on the time-frequency spread of the wavelet atoms, with the Heisenberg box being $s\sigma_t \times \frac{\sigma_\omega}{s}$. Thus, the uncertain area is constant, but low frequencies are well defined and spread out in time while high frequencies are poorly defined, but well localized in time.

This type of time-frequency representation is therefore well-suited for representing seismic signals and we use it to study the time-frequency characteristics of near and far offset trace.

Multiband analysis

The idea of decomposing seismic section into multiple frequency bands is not new (Yilmaz, 2001). Multiband analysis allows us to determine the signal-to-noise ratio and penetration depth for different frequencies. However, instead of using each bandpassed panel to help design an appropriate time-variant filter, we can process each such panel separately, including by 2D or 3D filters when necessary, and reassemble the denoised data by summing the processed panels. Such an approach is feasible if the summation of the unprocessed panels yields the original data up to the numerical precision. One option to achieve such decomposition is by utilizing a discrete wavelet transform (DWT), which is obtained by sampling time-frequency space of the CWT.

Each scale of a 1D DWT corresponds to a portion of the time-frequency space concentrated at specific frequency band. The maximum number of DWT decomposition levels depends on wavelet choice and length of a signal. By transforming a signal to the wavelet domain and reconstructing with coefficients corresponding to a specific scale, we decompose the input signal into multiple bands. Similarly to the Fourier transform, the only way to increase the resolution, or achieve a deeper decomposition level, is to record longer time series. Hence, we use a portion of continuously recorded seismic data for our analysis.

Dip filtering

In many cases it is possible to distinguish between events on the seismic record based on their apparent dip or velocity. Following Yu et al. (2017), we explore dip filtering in the complex wavelet domain. This transform is an enhancement to the real discrete wavelet transform offering attractive properties: near shift invariance and directional selectivity in 2D and higher dimensions (Selesnick et al., 2005). The former is of practical importance in the denoising applications. Setting wavelet coefficients to zero introduces oscillating artifacts in the denoised signal for large coefficients. These artifacts are significantly reduced if a shift-invariant transform is used since the signal estimation is averaged over translated wavelet bases (Mallat, 1999). The enhanced directional selectivity is a favorable feature for seismic data, allowing to better distinguish seismic events based on their dips.

Classical DWT is not shift-invariant and has limited directional selectivity. The complex wavelet transform ($\mathbb{C}$WT) can overcome these shortcomings by replacing the classical real wavelet with a complex, approximately analytic wavelet:

$$\psi_C(t) = \psi_r(t) + \mathrm{i}\psi_i(t), \tag{2}$$

where the real functions $\psi_r(t)$ and $\psi_i(t)$ are even and odd, respectively. Similarly, the $\mathbb{C}$WT utilizes a complex scaling function:

$$\phi_C(t) = \phi_r(t) + \mathrm{i}\phi_i(t), \tag{3}$$

with similar properties to the complex wavelet. The scaling function acts as a lowpass filter, while the wavelet function is a bandpass filter. Due to the one-sided frequency domain support of the analytic wavelets, the $\mathbb{C}$WT is able to distinguish between events of opposing dips. This property is important since the Fourier spectrum of seismic data is not always symmetric along the wavenumber axis.

One way of achieving an approximately analytic wavelet is by forming a slightly redundant frame such that both $\psi_r(t)$ and $\psi_i(t)$ form orthonormal or biorthogonal bases (Selesnick et al., 2005). An implementation following this approach is the dual-tree $\mathbb{C}$WT (Kingsbury, 2001) based on filter banks. The dual-tree $\mathbb{C}$WT can be computed using the infrastructure developed for classical DWT, though with specially designed filters (Selesnick et al., 2005). This makes the $\mathbb{C}$WT fast to compute ($\mathscr{O}(N)$ complexity) and 2^D times redundant tight frame (independent of the decomposition level) for $D-$dimensional signals.

The conventional interpretation of 2D $\mathbb{C}$WT suggests that the transform is sensitive to six angles: $\pm 15^\circ, \pm 45^\circ$ and $\pm 75^\circ$. However, for practical applications, it is important to understand how the physical dimensions of seismic data are mapped to specific scales and bands of the $\mathbb{C}$WT and their sensitivity to plane waves of different velocities. Figure 1 shows schematically the idealized support of the 2D complex wavelet coefficients for one quadrant of the Fourier space. We assume that data are sampled at 1ms in time and 1.25m in space, like in the examples demonstrated in the following section. The first level decomposition results in 3 details subspaces, traditionally linked to angles $15^\circ, 45^\circ$ and 75°. Physically these represent $(0.2-0.4)1/\mathrm{m} \times (0-250)\mathrm{Hz}$, $(0.2-0.4)1/\mathrm{m} \times (250-500)\mathrm{Hz}$ and $(0-0.2)1/\mathrm{m} \times (250-500)\mathrm{Hz}$, respectively. The remaining $(0-0.2)1/\mathrm{m} \times (0-250)\mathrm{Hz}$ band is a level 1 low frequency approximation - and it is this band that can be decomposed further, each time halving the bandwidth in frequency and wavenumber. Following this interpretation, we identify which scales and bands are most likely to have the majority of the energy corresponding to plane waves with specific velocities. Note in Figure 1 that slow surface waves (200 m/s) and sound waves (340 m/s) dominate at 15°. We demonstrate the denoising results leveraging that domain knowledge to suppress different types of noise present in seismic data by selectively zeroing the wavelet coefficients at specific bands and scales.

FIELD DATA ANALYSIS

We illustrate the methodology discussed here with field data acquired at the Colorado School of Mines geophysical field camp in a mountainous region of Colorado. Acquisition is done with a Vibroseis source using a 4-140Hz non-linear sweep, and the wireless receiver separation of 1.25m. We select a 33s window when the Vibroseis is close to the receivers. The nearest offsets are $\tilde{3}$m. Combined with the ultra-dense spatial sampling, this dataset enables detailed analysis of the seismic signal of interest generated by the non-linear sweep and the interfering noise (both source-generated and environmental).

Figure 2 shows the time-frequency characteristics of two traces,

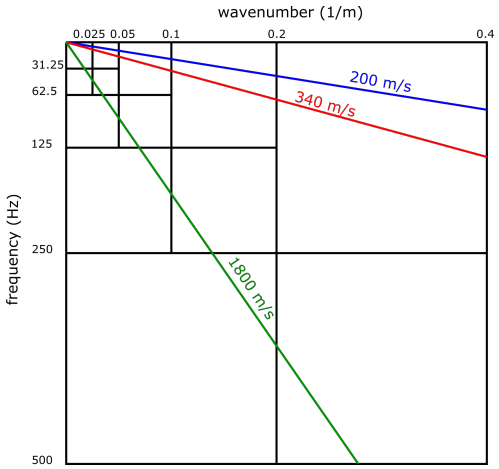

Figure 1: A schematic representation of the partitioning of the 2D Fourier space in the complex wavelet domain for temporal sampling of 1ms and spatial sampling of 1.25m. Different sizes of squares represent 4 decomposition scales and squares of the same size represent subbands within a scale. Slow planar events are distinct from fast planar events for all bands except for the coarsest scale approximation (top left corner).

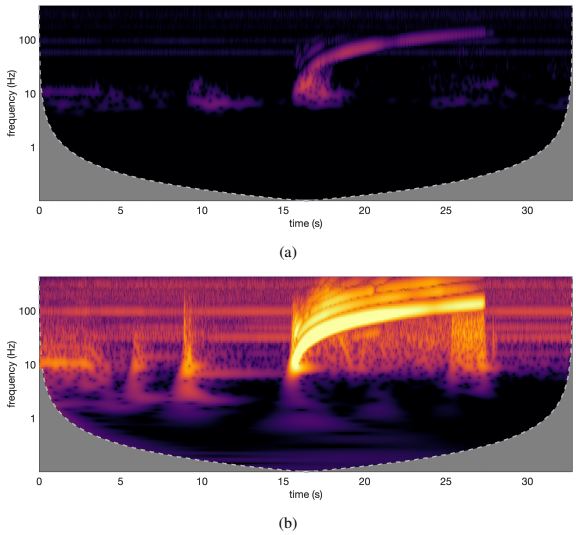

Figure 2: Logarithm of the magnitude of the CWT for (a) a 225m and (b) a 3m offset, both displayed on the same color scale. Note the high energy events before the sweep, monochromatic noise sources and harmonics of the sweep.

one near the source and one at an offset of 225m. Shaded regions correspond to areas where the continuous wavelet transform cannot provide reliable information, while the color represents logarithm of the magnitude of the CWT. Note that the energy generated by the Vibroseis source is mostly trapped in the near-source region, as indicated by cooler colors representing the sweep for the 225m offset trace. We also note several monochromatic noise sources. Figure 2(a) shows two distinct frequencies present at all times: around 60Hz and around 100Hz. In Figure 2(b), the 100Hz noise is also present and stronger while the 60Hz is no longer distinct. Furthermore, the near offset trace has monochromatic contributions from about 17Hz, 27Hz, 31Hz, 33Hz and 51Hz. This is consistent with results reported by Bagaini et al. (2014) who identify the mechanical components of the Vibroseis generating noise at specific frequencies. Time-frequency distribution for the two traces also reveals two high-energy events preceding the sweep (at about 6s and 9s), the increased mechanical noise during the last two seconds of sweeping, and strong harmonic distortion, especially near the source. The latter is known to cause the forerunner artifacts in the up-swept correlated data (Seriff and Kim, 1970) and is easier to address prior to the correlation by the appropriate time-varying filters.

The nature of high-energy events and mechanical noise during sweeping is best studied as a function of time and space. Figure 3 shows the same 33s of data as Figure 2 but in different frequency bands and at multiple offsets. The first 3.5s corresponds to the Vibroseis motion, with panel (c) indicating the starting and ending position. The motion itself generates slowly-propagating surface waves in the band 2-16 Hz. At 6s and 9s, the high-energy events depicted in Figure 2 occur and have similar characteristics to impact-generated seismic data. We interpret the first one as pressurization and the second as the coupling of the baseplate with the ground. Though rather narrow-band, the event at 9s can potentially be used to quality-check the correlation in the same band, provided that other source-related noise is suppressed. It also appears that the event at 9s has better low frequency content than the sweep, likely due to the harmonic distortion affecting sweep-generated data. The hardware solutions for suppressing the low frequency harmonics (Tellier and Ollivrin, 2019) are efficient, but only suitable if used during acquisition. Thus, for datasets with low frequency harmonic distortion, the pre-sweep data can prove valuable.

Panel (d) corresponding to 31-62 Hz reveals that the monochromatic 60Hz noise present in Figure 2(a) affects all receivers, is approximately constant phase and constant amplitude. The likely cause of this noise is the interference with powerlines which has to be suppressed to improve the reliability of broadband seismic data. Panels (d)-(f) indicate a periodic source which starts to move to the left during sweeping - that source is another vehicle, but its amplitudes are small enough to be of limited importance to the the correlated data.

The mechanical and acoustic noise generated by the Vibroseis is broadband and present at all times, but notably stronger during the sweep, peaking at the last two seconds of sweeping. Studying the moveout of the noise we conclude that it propagates with the velocity of surface waves for 0-62Hz and with velocity of the sound for higher frequencies. The noise is similar in terms of moveout and frequency composition for the duration of the whole sweep, with a significant amplitude increase when shaking 120-140Hz. We interpret that it might be caused by non-linear interactions between baseplate and the soil, baseplate flexure and limitations in the Vibroseis' hydraulics system such as response time of pump to changes in demands for flow output (Sallas, 2010). This noise is some-

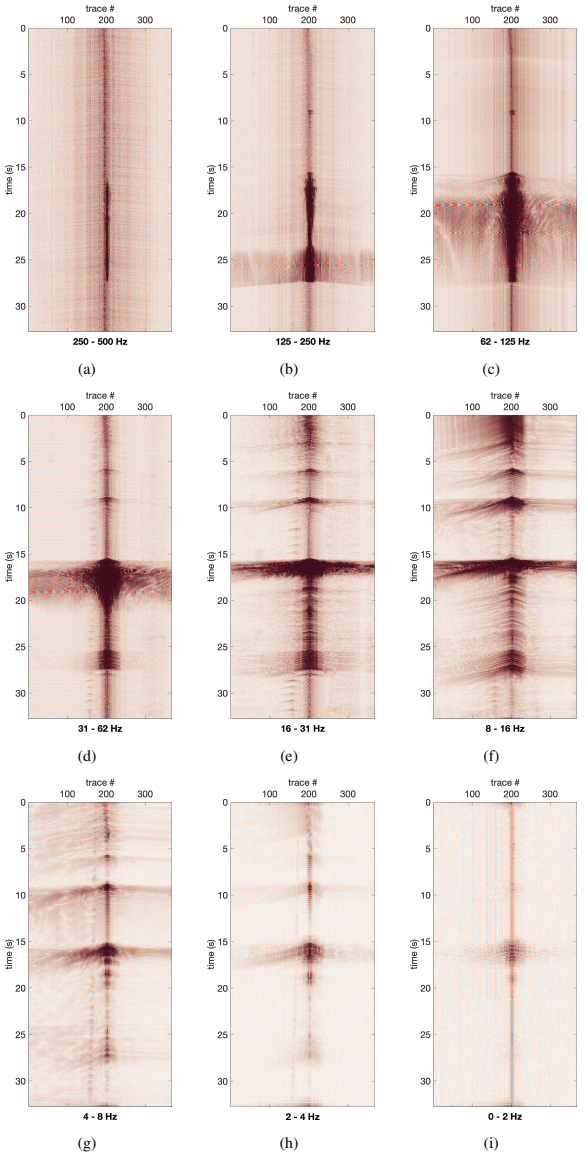

Figure 3: Multiscale decomposition of the seismic data. Reliable information can be extracted for frequencies below 10Hz, the natural frequency of the used geophones.

times referred to as 'chimney noise' in the correlated data (Bagaini et al., 2014) and completely obscures any geologic information in the immediate vicinity of the source.

We use the observed noise characteristics to inform the $\mathbb{C}$WT denoising on the data panels in Figure 3. The denoising strategy hinges on zeroing or thresholding the wavelet coefficients at specific bands and scales. We assess the results of the denoising by looking at correlation without processing, correlation preceded by denoising and the data difference between these two, as shown in Figure 4. The raw correlated data in panel (a) are dominated by the surface waves, which are successfully suppresed in panel (b). The difference plot in panel (c) reveals that the suppressed noise also includes airwaves and

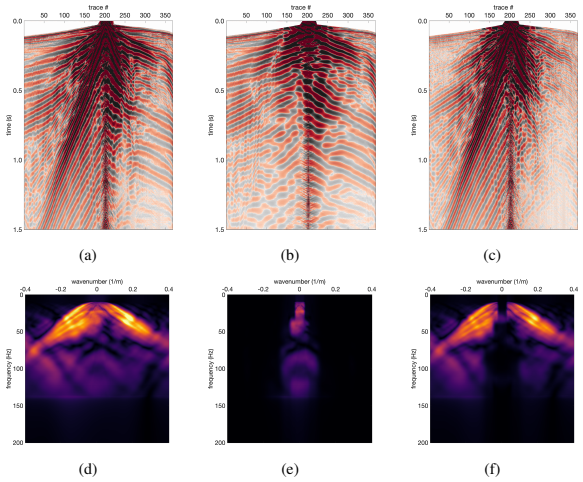

Figure 4: (a) Data correlated without denoising, (b) after denoising and (c) difference between (a) and (b). (d)-(f) are the corresponding F-K spectra on the same color scale. $\mathbb{C}$WT denoising acts as a dip filter, preserving high velocity events.

big portion of source-generated noise. Though not shown here, examination of data around 60Hz confirmed suppression of powerline interference. Panels (d)-(e) depict the F-K spectra corresponding to (a)-(c). It is clear that $\mathbb{C}$WT denoising works as expected, targeting seismic events of specific frequencies and velocities, similarly to the classical F-K filter. The denoised data preserve the original bandwidth and only suffer from minor filtering artifacts at near offsets and early times.

CONCLUSIONS

The informed use of wavelet-based transforms provides a wealth of information which help to characterize the signals in seismic data. Long acquisition time series improve the definition of low frequency content and indicate the potential value of pre-sweep data. By linking the complex wavelet domain to the physical dimensions of seismic data, we are able to predict which scales and bands of the transform contain information about specific plane wave-like events, providing an important link to the well-understood Fourier domain. The domain knowledge can be used to suppress specific portions of data, such as surface waves, powerline interference, source-generated mechanical noise and air waves. The framework presented in this paper is a powerful tool for noise suppression in land seismic data and has a natural extension to 3D.

ACKNOWLEDGMENTS

We acknowledge Dawson and Sercel for providing equipment and technical support at the CSM Geophysical Field Camp. We also thank GTI for allowing us to test wireless nodes and conduct dense sampling experiments. SEG provided partial financial support of the Field Camp. We also acknowledge the CSM undergraduate students who conducted the acquisition.

REFERENCES

Abma, R., D. Howe, M. Foster, I. Ahmed, M. Tanis, Q. Zhang, A. Arogunmati, and G. Alexander, 2015, Independent simultaneous source acquisition and processing: Geophysics, **80**, WD37–WD44.

Baeten, G., J. W. de Maag, R.-E. Plessix, R. Klaassen, T. Qureshi, M. Kleemeyer, F. t. Kroode, and Z. Rujie, 2013, The use of low frequencies in a full-waveform inversion and impedance inversion land seismic case study: Geophysical Prospecting, **61**, 701–711.

Bagaini, C., 2006, Overview of simultaneous vibroseis acquisition methods, *in* SEG Technical Program Expanded Abstracts 2006: Society of Exploration Geophysicists, 70–74.

Bagaini, C., M. Laycock, C. Readman, E. Coste, and C. Anderson, 2014, Seismo-acoustic characterization of a seismic vibrator, *in* SEG Technical Program Expanded Abstracts 2014: Society of Exploration Geophysicists, 25–29.

Berkhout, A. J. G., 2008, Changing the mindset in seismic data acquisition: The Leading Edge, **27**, 924–938.

Gabor, D., 1946, Theory of communication: J. IEE (London), **93**.

Ghosh, S. K., 2000, Limitations on impedance inversion of band-limited reflection data: Geophysics, **65**, 951–957.

Kabir, M. N., and D. Verschuur, 1995, Restoration of missing offsets by parabolic Radon transform: Geophysical Prospecting, **43**, 347–368.

Kapoor, J., C. Stork, and M. Egan, 2005, Benefits of low frequencies for subsalt imaging, *in* SEG Technical Program Expanded Abstracts 2005: Society of Exploration Geophysicists, 1993–1996.

Kingsbury, N., 2001, Complex wavelets for shift invariant analysis and filtering of signals: Applied and computational harmonic analysis, **10**, 234–253.

Mallat, S., 1999, A wavelet tour of signal processing: Elsevier.

Morlet, J., G. Arens, E. Fourgeau, and D. Giard, 1982a, Wave propagation and sampling theory—Part II: Sampling theory and complex waves: Geophysics, **47**, 222–236.

Morlet, J., G. Arens, E. Fourgeau, and D. Glard, 1982b, Wave propagation and sampling theory—Part I: Complex signal and scattering in multilayered media: Geophysics, **47**, 203–221.

Ross, C. P., and D. L. Kinman, 1995, Nonbright-spot AVO: Two examples: Geophysics, **60**, 1398–1408.

Sallas, J. J., 2010, How do hydraulic vibrators work? a look inside the black box: Geophysical Prospecting, **58**, 3–18.

Selesnick, I. W., R. G. Baraniuk, and N. G. Kingsbury, 2005, The dual-tree complex wavelet transform: IEEE Signal Processing Magazine, **22**, 123–151.

Seriff, A., and W. Kim, 1970, The effect of harmonic distortion in the use of vibratory surface sources: Geophysics, **35**, 234–246.

Tellier, N., and G. Ollivrin, 2019, Low-frequency Vibroseis: current achievements and the road ahead?: First Break, **37**, 48–54.

Verschuur, D. J., A. Berkhout, and C. Wapenaar, 1992, Adaptive surface-related multiple elimination: Geophysics, **57**, 1166–1177.

Xu, Y., J. Xia, and R. D. Miller, 2006, Quantitative estimation of minimum offset for multichannel surface-wave survey with actively exciting source: Journal of Applied Geophysics, **59**, 117–125.

Yilmaz, Ö., 2001, Seismic data analysis: Processing, inversion, and interpretation of seismic data: Society of Exploration Geophysicists.

Yu, Z., R. Abma, J. Etgen, and C. Sullivan, 2017, Attenuation of noise and simultaneous source interference using wavelet denoising: Geophysics, **82**, V179–V190.

Zhang, L., and E. Slob, 2020, A field data example of marchenko multiple elimination: Geophysics, **85**, S65–S70.